Solutions to range-dependent benchmark problems by the finite-difference method

Ralph A. Stephen
Woods Hole Oceanographic Institution, Woods Hole, Massachusetts 02543

(Received 28 October 1988; accepted for publication 3 October 1989)

An explicit second-order finite-difference scheme has been used to solve the elastic-wave equation in the time domain. Solutions are presented for the perfect wedge, the lossless penetrable wedge, and the plane parallel waveguide that have been proposed as benchmarks by the Acoustical Society of America. Good agreement with reference solutions is obtained if the media is discretized at 20 gridpoints per wavelength. There is a major discrepancy (up to 20 dB) in reference-source level because the reference solutions are normalized to the source strength at 1 m in the model, but the finite-difference solutions are normalized to the source strength at 1 m in a homogeneous medium. The finite-difference method requires computational times between 10 and 20 h on a super minicomputer without an array processor. The method has the advantage of providing phase information and, when run for a pulse source, of providing insight into the evolution of the wave field and energy partitioning. More complex models, including velocity gradients and strong lateral heterogeneities, can be solved with no additional computational effort. The method has also been formulated to include shear wave effects.

PACS numbers: 43.30.Bp

INTRODUCTION

In order to test various numerical schemes for range-dependent problems in ocean acoustics, the Acoustical Society of America has defined a set of benchmark models. These were established at the 1986 Fall meeting in Anaheim, and preliminary results were presented at the 1987 Spring meeting in Indianapolis. The models are presented by Jensen and Ferla.[1]

In this paper, we give solutions to the benchmark models using the finite-difference method applied to the two-way elastic wave equation. This code was developed to study strong scattering from rough liquid–solid interfaces and lateral heterogeneities beneath the seafloor.[2–5] It allows for multiple scattering, the effects of shear wave and density variations, and either pulse or continuous wave sources. The proposed benchmark models are purely acoustic; with no shear wave effects and hence are a subset of the class of models that the code was intended to address. However, it is important that the method solve these problems accurately in order to demonstrate its validity for range-dependent problems. Similar codes have already been tested for accuracy for laterally homogeneous liquid–solid interfaces[2] and good results were obtained. The next step in the benchmark process will be to include shear wave effects in range-dependent models.

I. THE FINITE-DIFFERENCE METHOD

A. The wave equation and differencing scheme

We solve the two-way elastic wave equation for compressional and vertically polarized shear waves (*P-SV*) in two dimensions that can be written as a hyperbolic system of coupled equations, in Cartesian coordinates (x,z):

$$
\begin{aligned}
\rho\frac{\partial^2 u_x}{\partial t^2} &= \frac{\partial \tau_{xx}}{\partial x} + \frac{\partial \tau_{xz}}{\partial z},\\
\rho\frac{\partial^2 u_z}{\partial t^2} &= \frac{\partial \tau_{xz}}{\partial x} + \frac{\partial \tau_{zz}}{\partial z},\\
\tau_{xx} &= (\lambda+2\mu)\frac{\partial u_x}{\partial x} + \lambda\frac{\partial u_z}{\partial z},\\
\tau_{zz} &= (\lambda+2\mu)\frac{\partial u_z}{\partial z} + \lambda\frac{\partial u_x}{\partial x},\\
\tau_{xz} &= \mu\left(\frac{\partial u_x}{\partial z} + \frac{\partial u_z}{\partial x}\right),
\end{aligned}
\tag{1}
$$

where (u_x,u_z) is the particle-displacement vector, τ_{xx} and τ_{zz} are normal stresses, and τ_{xz} is tangential stress. The density (ρ) and Lamé's parameters (λ and μ) are functions of range (x) and depth (z). In cylindrical coordinates (r,z), the equations become

$$
\begin{aligned}
\rho\frac{\partial^2 u_r}{\partial t^2} &= \frac{1\partial}{r\partial r}(r\tau_{rr}) - \frac{1}{r}\tau_{\phi\phi} + \frac{\partial}{\partial z}\tau_{rz},\\
\rho\frac{\partial^2 u_z}{\partial t^2} &= \frac{1\partial}{r\partial r}(r\tau_{rz}) + \frac{\partial}{\partial z}\tau_{zz},\\
\tau_{rr} &= (\lambda+2\mu)\frac{\partial u_r}{\partial r} + \frac{\lambda}{r}u_r + \lambda\frac{\partial u_z}{\partial z},\\
\tau_{\phi\phi} &= \lambda\frac{\partial u_r}{\partial r} + \frac{(\lambda+2\mu)}{r}u_r + \frac{\lambda\partial u_z}{\partial z},\\
\tau_{zz} &= \lambda\frac{\partial u_r}{\partial r} + \frac{\lambda}{r}u_r + (\lambda+2\mu)\frac{\partial u_z}{\partial z},\\
\tau_{rz} &= \mu\left(\frac{\partial u_z}{\partial r} + \frac{\partial u_r}{\partial z}\right).
\end{aligned}
\tag{2}
$$

Stephen[6] reviews many approaches to taking finite differences of the system (2). For liquid–solid interfaces the

 0001-4966/90/041527-08$00.80

scheme of Madariaga[7] and Virieux[8] is promising both for stability and accuracy. They solve the equivalent first-order system to Eq. (1) or (2) in terms of particle velocity and stress. The five (or six) field variables $(\partial u_r/\partial t, \partial u_z/\partial t, \tau_{xx}, \tau_{zz}, \tau_{xz})$ and three independent variables (ρ, λ, μ) are defined on a staggered grid as in Fig. 1. In order to reduce memory requirements, we solve Eqs. (1) and (2) directly for displacement. We only save the two particle displacements at each grid point but compute the next time step using stress as a temporary, intermediate variable. We then use traditional, centered, finite differences. For example, consider the first equation in system (1):

$$\rho \frac{\partial^2 u_x}{\partial t^2} = \frac{\partial \tau_{xx}}{\partial x} + \frac{\partial \tau_{xz}}{\partial z}.$$

For accuracy and stability, all terms of the equation should be defined at the same point in space and in time:

$$\rho \frac{\partial^2 u_x}{\partial t^2}(m,n,k) \approx \rho(m,n)\{[u_x(m,n,k+1) - 2u_x(m,n,k) + u_x(m,n,k-1)]/\Delta t^2\}, \quad (3)$$

$$\frac{\partial \tau_{xx}}{\partial x}(m,n,k) \approx \frac{\tau_{xx}(m+1/2,n,k) - \tau_{xx}(m-1/2,n,k)}{\Delta x},$$

$$\frac{\partial \tau_{xz}}{\partial z}(m,n,k) \approx \frac{\tau_{xz}(m,n+1/2,k) - \tau_{xz}(m,n-1/2,k)}{\Delta z}.$$

[We assume here that Δx, Δz, and Δt are the grid increments in range, depth, and time and that m, n, and k are the corresponding indices, i.e., $u(m,n,k) = u(m\Delta x, n\Delta z, k\Delta t)$.] If vertical and horizontal displacements are known at present and past time steps (k and $k-1$), then Eqs. (3) can be solved explicitly in the time domain for the displacements at the future time step ($k+1$).

Also, to improve efficiency, for the models shown here, we have removed the terms that are dependent on shear modulus (the shear-wave velocity and tangential stress). Equations (1) and (2) then reduce to acoustic-wave equations with range- and depth-dependent compressional wave velocity and density.

We compute pressure (p) from displacements using

$$p = -\lambda\left(\frac{\partial u_x}{\partial x} + \frac{\partial u_z}{\partial z}\right), \quad (4)$$

for Cartesian coordinates, and

$$p = -\lambda\left(\frac{1\partial(ru_r)}{r\,\partial r} + \frac{\partial u_z}{\partial z}\right), \quad (5)$$

for cylindrical coordinates.

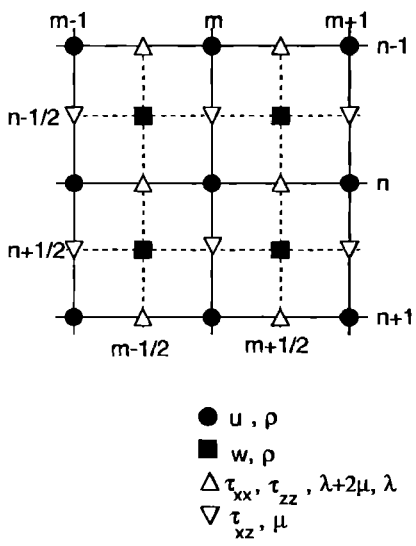

FIG. 1. Horizontal and vertical displacements (u,w), elastic parameters (λ, μ, and $\lambda + 2\mu$) and density (ρ) are defined at locations offset by half a grid interval from one another as shown. This offset leads to a stable finite-difference scheme based on second-order-centered finite differences that has favorable dispersion properties over a wide range of Poisson's ratio.

B. Geometry

Depending on the application, we can use either Cartesian coordinates or cylindrical coordinates. Because of the symmetry assumed to reduce the above systems [Eqs. (1) and (2)] from three dimensions to two, an omnidirectional source in Cartesian coordinates is actually a line source along the y axis and any range-dependent structure in cylindrical coordinates will wrap around the axis of symmetry like an annulus. In cylindrical coordinates, the point source must be on the axis of symmetry. Otherwise, it would represent a "ring" or "doughnut" source. So, an omnidirectional source in cylindrical coordinates (on the axis of symmetry) is solving a full three-dimensional problem for a point source with cylindrically symmetrical range-dependent structure. An omnidirectional source in Cartesian coordinates is solving either the line source problem in three dimensions or the point source problem in two dimensions. In either case, there is inherent dispersion in the solution and waveforms distort with range even for perfectly elastic, homogeneous media. This inherent dispersion should not be confused with the grid dispersion of finite-difference schemes discussed further below.

C. Initial and boundary conditions

For the models presented here, the initial conditions are zero displacement and velocity everywhere on the grid.

The top boundary is a free surface of a liquid ($\tau_{xx} = \tau_{zz} = 0$). This is simulated by introducing an imaginary row along the top of the finite-difference grid at $n = 1$. The free surface is at $n = 2$. The horizontal displacement at the free surface is set identically to zero [$u_r(m,2,k) \equiv 0$] and the vertical displacement at the imaginary row is set equal to the vertical displacement just below the free surface [$u_z(m,1+\frac{1}{2},k) = u_z(m,2+\frac{1}{2},k)$]. These conditions assure that the stress will vanish.

The left-hand edge for the models in Cartesian coordinates is an absorbing boundary based on the second-order scheme of Clayton and Engquist.[9] It takes a paraxial approximation normal to the boundary in order to predict what the displacements will be on the left edge. For the models in cylindrical coordinates, the left-hand edge is an axis of symmetry.

The right-hand edge for the models in both coordinate

systems is an absorbing boundary based on the second-order scheme of Clayton and Engquist[9] as above.

We normally use the same paraxial approximation scheme at the bottom boundary of the grid. However, at the long time intervals required for some of the benchmarks, this scheme was unstable. We used instead an absorbing region 50 grid points deep in which we solved the "telegraph" equation.[10,11] This attenuates the energy with an operator based on the first-time derivative. For example, the left-hand side of the first equation in system (1) becomes

$$\rho\left(\frac{\partial^2 u_x}{\partial t^2}+\alpha\frac{\partial u_x}{\partial t}\right). \tag{6}$$

In order to prevent reflections from this region, we increased the attenuation parameter, (α), gradually with depth according to the function:

$$\begin{aligned}\alpha &= 0, \quad z<z_{\text{ref}}\\ &= a_1+(a_2-a_1)\{\cos[\pi(1+a_3)]+1\}, \quad z>z_{\text{ref}},\end{aligned} \tag{7}$$

where $a_1=0.001$, $a_2=0.025$, $a_3=(z-z_{\text{ref}})/(z_{\max}-z_{\text{ref}})$, z_{ref} is the top of the absorbing region and $z_{\max}$ is the bottom of the grid.

For sharp boundaries within the grid, we did not specifically code boundary conditions. The effects of the boundary can be adequately treated by the implied derivatives of the medium parameters in Eqs. (1) and (2). This is important for further applications of the method where boundaries of arbitrary shape could be introduced. If boundary conditions were specifically coded, the code would change depending on the shape of the boundary.

D. The source

The source is introduced into the grid as horizontal and vertical forces.[12] Previous applications of the code used pulse sources in order to study multipathing and scattering in sea bottom structure. Continuous wave sources are used in the benchmarks, and these were synthesized by using a continuous wave as the source function and running the code long enough that steady state was reached at all of the receivers. Obviously, this is a cumbersome way to solve a continuous wave problem. However, it has the advantages (i) of automatically including phase information (not assigned for the benchmark problem) and (ii) of being able, with the same code, to run a pulse source and to track the energy partitioning as a function of time in the model.

In order to calibrate the propagation loss curves for source strength, we ran a homogeneous model for both the Cartesian and cylindrical geometry codes. We then computed the power at a line of receivers away from the source in the same fashion as for the benchmark models. These power-loss curves (power in dB versus the logarithm of the range) were then extrapolated back to a range of 1 m to get the reference source strength. (These curves were linear with slopes of -10 dB/log r and -20 dB/log r for Cartesian and cylindrical geometry, respectively.) The power results for the benchmark models were then corrected for this value to get loss in dB relative to the source strength at 1 m.

E. Stability and dispersion

Virieux[8] gives a necessary stability criteria for the scheme outlined above. For a given space increment (Δx), the time increment (Δt) must satisfy

$$\Delta t<\frac{\Delta x}{\sqrt{2}V_{p\max}} \tag{8}$$

where $V_{p\max}$ is the maximum compressional wave velocity in the model. This relationship is based on analysis of the scheme for homogeneous media. However, the stability condition for homogeneous media is only a necessary condition for heterogeneous media.[6] Sufficient conditions for heterogeneous media are not known. Some codes are unstable for heterogeneous media even though the stability criteria for homogeneous media is satisfied locally. Tests of this scheme indicate that it is stable over a broad range of contrasts in Poisson's ratio at sharp, rough interfaces.

Stability at absorbing boundaries is another issue that is not well understood. The absorbing boundary formulation based on the paraxial approximation used above absorbs the initially incident compressional and shear waves. However, if run to sufficiently long times, as was required for these benchmark models, instabilities arose at the boundaries and rendered the results unusable. The combination of a paraxial approximation on the right-hand edge, and a telegraph equation region along the bottom boundary has given acceptable results for these models.

Any finite-difference scheme has numerical dispersion in which velocity across the grid becomes frequency dependent. Because the effective grid spacing normal to a wavefront varies with direction, the grid dispersion is anisotropic.[12,13] The effect of grid dispersion introduces inaccuracies in the results. Analysis of the grid dispersion for the above scheme in homogeneous media[8] shows that: (i) the dispersion relation for P waves is independent of Poisson's ratio; (ii) the numerical S wave always travels slower than the true S wave; and (iii) grid dispersion for S waves does not degrade as Poisson's ratio approaches 0.5 (very slow S waves). For acceptable grid dispersion, there should be at least ten grid points per wavelength. In previous work, we have found this acceptable for models out to 100 wavelengths. For the models shown here, we used 20 grid points per wavelength. Grid dispersion yields progressively less accurate results as the wave propagates to longer times and ranges. For the benchmark models, we ran the code to longer durations than usual to get the steady-state continuous-wave response and thus required more dense sampling. Even finer grid spacing may improve the accuracy for some models, but this was not carried out in this study.

F. Attenuation

It is difficult to obtain a stable formulation in the time domain for the wave equation with general frequency-dependent attenuation.[14] However, the telegraph equation, used for the bottom boundary, does have a stable formulation. For the continuous wave problem posed in the benchmarks, we can introduce attenuation into the bottom by using the telegraph equation with the appropriately selected

parameter α. For a homogeneous, acoustic medium with attenuation, system (1) and relation (6) reduce to the telegraph equation for pressure (p):

$$\frac{\partial^2 p}{\partial t^2} + \alpha \frac{\partial p}{\partial t} = c^2 \nabla^2 p, \tag{9}$$

where $c = (\lambda/\rho)^{1/2}$. If α is small, the solution to this equation is $\exp[-\alpha r/(2c)]g(r-ct)$ which is a damped, traveling wave as required. The coefficient α in this equation is related to the quality factor Q and the amplitude decay per wavelength by

$$\alpha = \omega/Q = -2f\log[p(r+\lambda)/p(r)], \tag{10}$$

where f is frequency, λ is wavelength, log is the natural logarithm, and $\omega = 2\pi f$. So, for continuous wave problems and small attenuations, we can use the telegraph equation to introduce attenuation into the finite-difference code.

III. BENCHMARK RESULTS

A. The wedge with a pressure-release bottom

The geometry for the wedge models is shown in Fig. 2. A 25-Hz continuous wave source is located at zero range and middepth in 200 m of water and the bottom shallows at a slope of 1 in 20 up to the apex at 4 km. Horizontal arrays of pressure receivers are located at depths of 30 and 150 m.

This problem is particularly challenging for a numerical scheme because of the highly oscillatory nature of the propagation-loss curve. The separation between minima in the curve is about 40 m and the wavelength of 25-Hz sound in water is about 60 m. So the propagation-loss curve, the amplitude envelope of the wave field, oscillates more in space than the free-space wave field itself. In the context of finite differences, we normally sample at 10 grid points per wavelength but in order to sample this solution adequately, we used 24 grid points per wavelength.

For the bottom of the wedge, we set the parameters on the Cartesian grid to represent the sloping bottom stepwise (Fig. 3). By sampling the grid finely enough, we should obtain the solution for the actual sloping bottom case. The effect of the free surface at the bottom was simulated by setting the compressional wave speed to zero, and holding the density constant at those grid points below the stepwise interface. [The acoustic wave equation in terms of displacement is $\rho \ddot{u}_j = \tau_{ij,j}$ and, $\tau_{ii} = \lambda u_{j,j}$ where u_j is the jth component of displacement and τ_{ii} is the principle normal stress (shear stresses being zero). Setting velocity $(\lambda/\rho)^{1/2}$ equal to zero and holding density constant, sets τ_{ii} to zero by default since λ is automatically zero.]

Our code is based on a time-domain solution to the wave equation. In order to solve the continuous wave problem, we start a sine wave at the source location and carry out the computations until steady state is reached at the receiver points of interest. Figure 4 shows how the time series at the horizontal line of receivers evolve. The onset of the wave field propagates up the wedge and reflects back down, generating the complex interference pattern. Once steady state is reached at a receiver, we compute the propagation loss by taking the root mean square of the amplitude values for pressure for four cycles and dividing by the normalization factor for the source strength.

The results for the wedge with a pressure-release bottom are compared with the COUPLE (two-way) solution[1] in Fig. 5. There is an obvious offset in the reference level. In the COUPLE (two-way) solution, the reference level was chosen at 1 m from the source in the actual wedge model. (It is not clear how this was obtained since the COUPLE results were inaccurate at less than 100 m.) In the finite-difference solution, the reference level was chosen at 1 m from the source in a homogeneous medium. Since the grid spacing was 2.5 m and the field was oscillating rapidly, we had no way of directly computing the field at 1 m for the wedge model. For many applications, the source strength in homo-

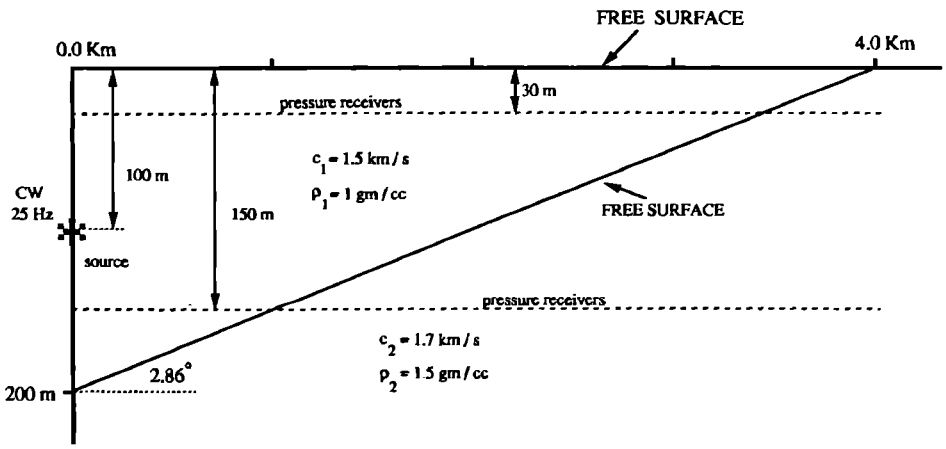

FIG. 2. The geometry for the wedge models is defined.

Case I stress release on bottom - line source in Cartesian co-ordinates (left boundary is a radiation condition)

Case II 0 attenuation -] point source in cylindrical co-ordinates (solution for an inverted cone in 3-D)

Case III 1/2 db/λ attenuation -]

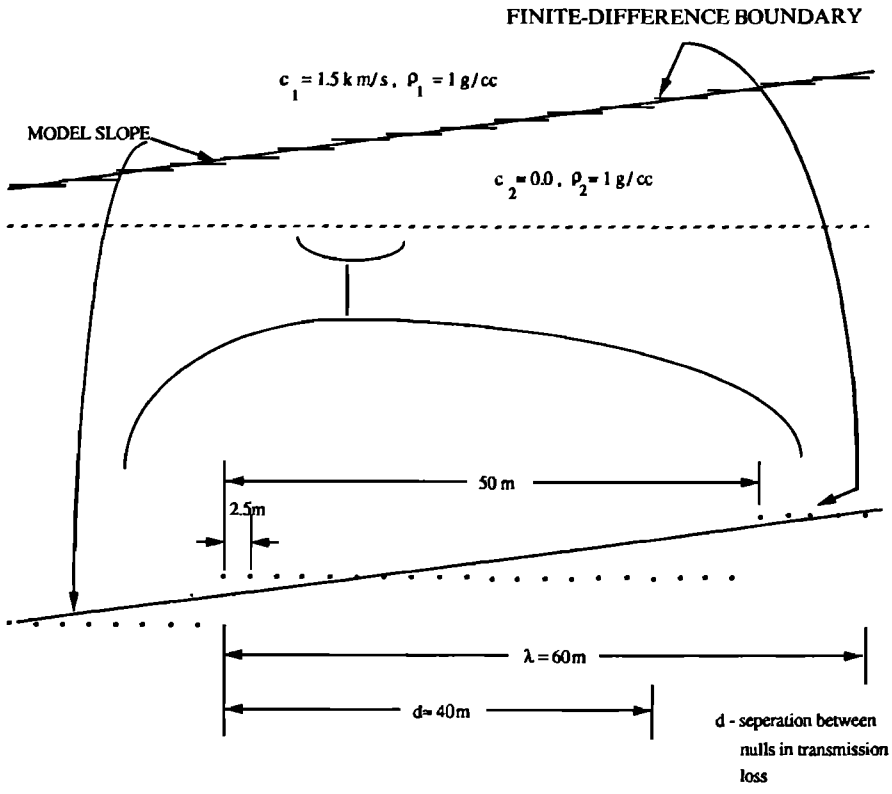

FIG. 3. The detailed view of the bottom boundary of the wedge shows how the finite-difference grid approximates the sloping boundary stepwise. The wavelength (λ) and the separation between nulls in the propagation-loss curve for the perfect wedge (d) are shown for comparison.

geneous media is more meaningful since it is independent of the model. It can be used to compare propagation-loss levels between models and also to compare modeling results with laboratory or field experiments.

The general character of the two curves in Fig. 5 is similar, but there are small offsets in the locations of the peaks and nulls. This could be due to the coarseness of approximating the sloping bottom by a stepwise function (Fig. 3). The COUPLE solution used 500 steps over the 4 kms, but the finite-difference solution used only 80 steps.

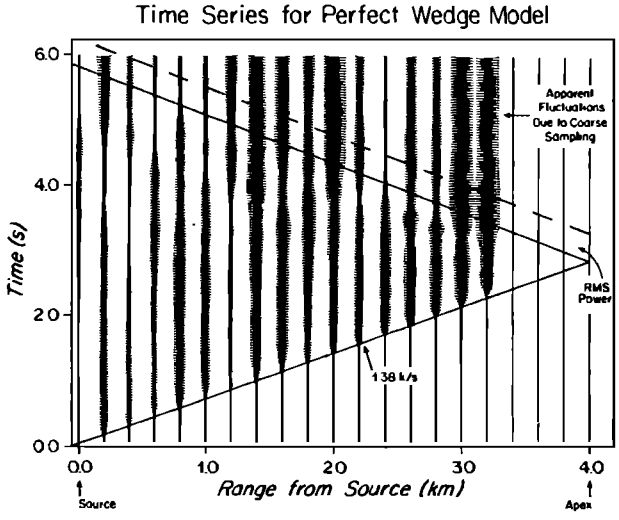

FIG. 4. This figure shows the time-domain response of the finite-difference solution for the line of receivers at 30-m depth. The 25-Hz continuous wave source is initiated and the resulting wave propagates up into the wedge and back again. The steady-state response was computed for a window just behind the retrograde line (labeled rms power).

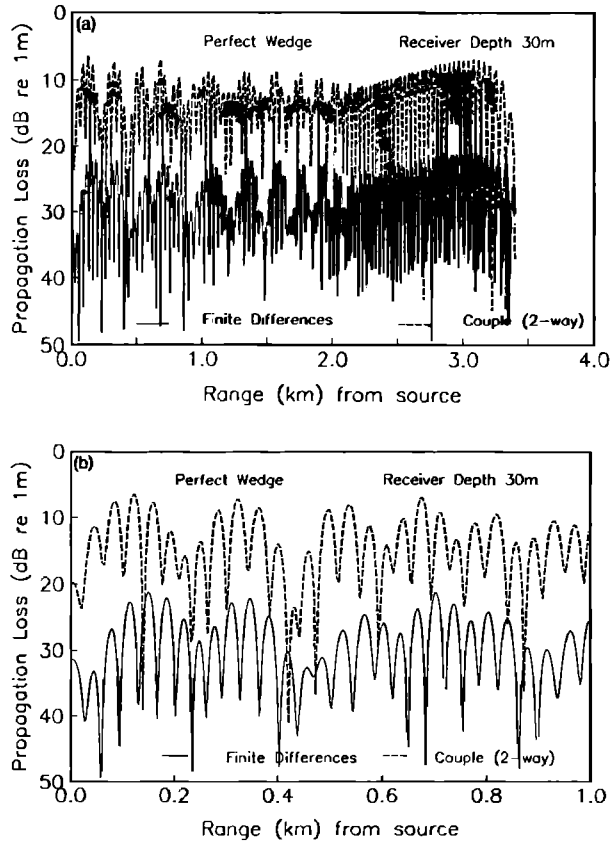

FIG. 5. Propagation-loss curves for the perfect wedge. (a) The benchmark solution and (b) an expanded view of the first 1.0 km. The upper curve in each case is the COUPLE (two-way) solution of Jensen and Ferla[1] and the lower curve is the finite-difference result. The 20-dB offset in curves is due to a different definition of reference-source level in each case. The general character of the solution is similar but the specific location of peaks and troughs varies.

The contoured field solution for this model (Fig. 6) shows more clearly the separation of the wedge into three regions, one region each corresponding to three-mode, two-mode, and one-mode propagation. As the wedge gets shallower, progressively fewer modes are supported by the waveguide.

B. Wedge with a lossless penetrable bottom

The solutions in this case were computed in a similar fashion to the previous model. However, a point source in cylindrical geometry was employed. The problem corresponds to a point source over an inverted cone. Time and space increments were identical to the previous model, but total model dimensions varied. The left-hand edge is an axis of symmetry and the bottom and right edges are absorbing boundaries to handle the energy penetrating the bottom.

The solutions are given in Fig. 7. Again, good agreement with coupled mode solutions (two-way) is obtained except for the reference level. The agreement is very good for the receivers at 30 m. The agreement is not very good at 3-km range for the lower level of receivers. The very low field values here are not well represented. Further study is required to fully resolve this issue.

The contoured field solution is shown in Fig. 8, and this also agrees quite favorably with the coupled-mode results (see Fig. 8 in Jensen and Ferla[1]).

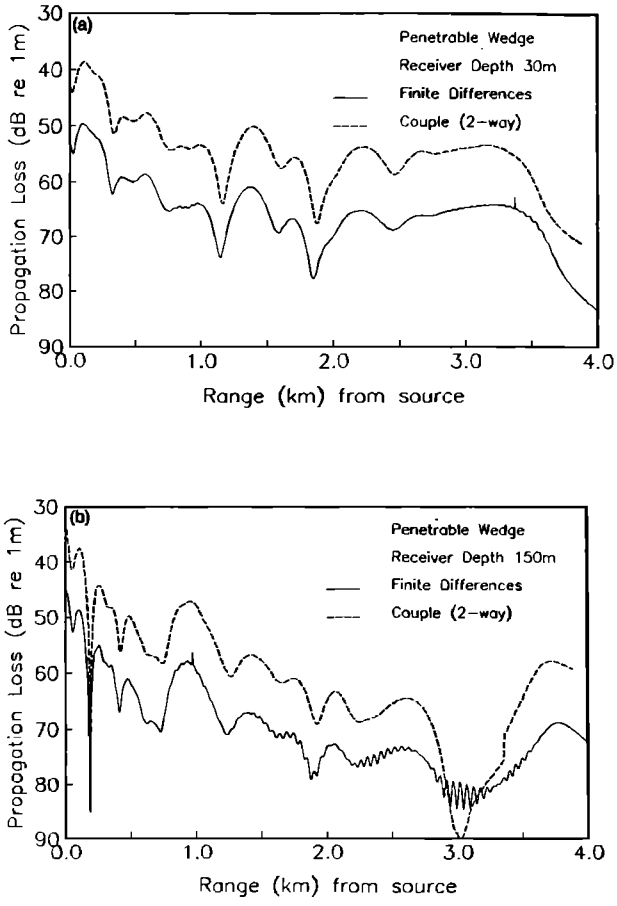

FIG. 7. Propagation-loss curve for the lossless penetrable wedge at (a) 30-m depth and (b) 150-m depth. The upper curve in each case is the COUPLE (two-way) solution of Jensen and Ferla[1] and the lower curve is the finite-difference result. The solutions at 30-m depth agree very well except for the offset in reference source level. The solutions at 150 m also agree well above 70 dB but lower values are poorly represented by the finite-difference method.

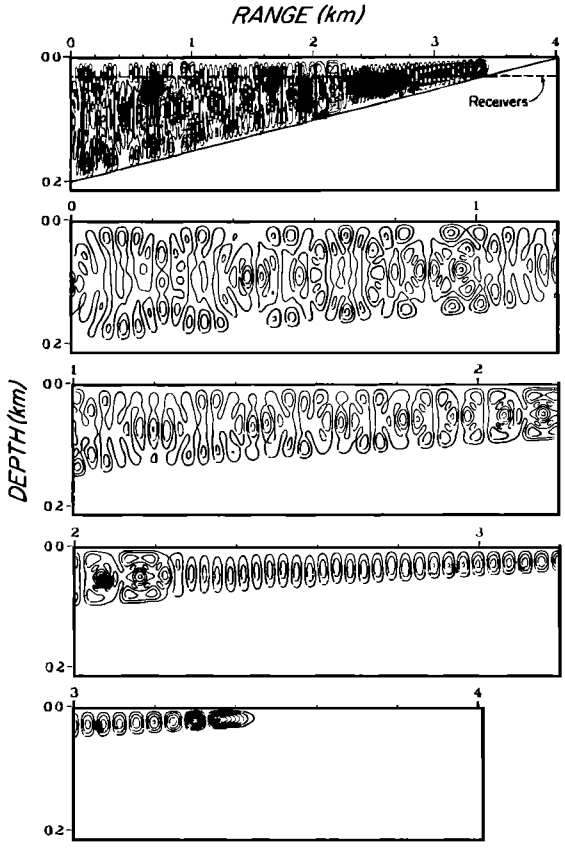

FIG. 6. Contoured-field solution for the perfect wedge. The top frame is the complete field and the lower frames show expanded views. The three regions of one-mode (2.2–3.4 km), two-mode (1.0–2.2 km), and three-mode (0–1.0 km) propagation can be identified.

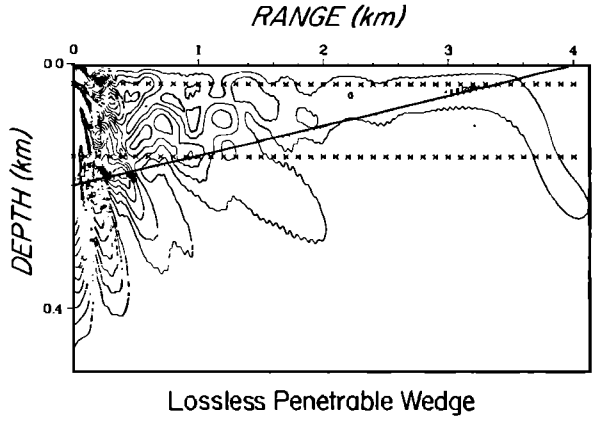

FIG. 8. Contoured-field solution for the lossless penetrable wedge. Contour interval is 3 dB. The penetration of energy into the bottom as the modes cutoff is clearly demonstrated. The solutions agree well within the first 500 m, where the lateral heterogeneity occurs. It is not clear why there are large discrepancies beyond this range.

C. Wedge with a lossy penetrable bottom

In order to introduce loss into the bottom, we tried the telegraph-equation approach as outlined in Sec. I(F) above. For a loss of 0.5 dB/wavelength, the attenuation parameter α would be -2.88 (for a Q of 54.6). We tried this, but the code was unstable at the water–sediment boundary. Since 2.88 is not a small value, approximating attenuation using the telegraph equation is inappropriate. We conclude that this approach should not be taken for large attenuations.

D. Plane-parallel waveguide

The plane-parallel waveguide problem is defined in Jensen and Ferla.[1] The depth of the waveguide is 500 m. The sound speed varies in both range and depth within the waveguide. The rigid–bottom boundary was simulated by keeping the displacements zero in the calculations. The source frequency is 25 Hz. The finite-difference solution for a source and receivers at 250-m depth is given in Fig. 9 for the omnidirectional point source case.

The reference level of the two curves is within 5 dB in this case, and the solutions at less than 700 m are in very good agreement. However, beyond 700 m, the COUPLE (one-way) solution is oscillating much more rapidly than the finite-difference curve. The COUPLE (one-way) solution used as the reference here included 17 source modes. The finite-difference solution agrees better with the COUPLE (two-way) solution using 10 source modes given in Fig. B10-A of Jensen and Ferla.[1] The actual analytical solution for this problem was not available at the time of submission. Since 24 grid points per wavelength should be adequate for this problem, we believe the finite-difference solution is correct. We should run a finer grid spacing to confirm convergence.

The contoured field solution for this problem is given in Fig. 10.

III. COMPUTATIONAL PERFORMANCE

The computational performance for the three models given in this paper is summarized in Table I. The perfect-wedge and plane-parallel waveguide models were run on a VAX 8800 with 48 Mbytes of random-access (primary)

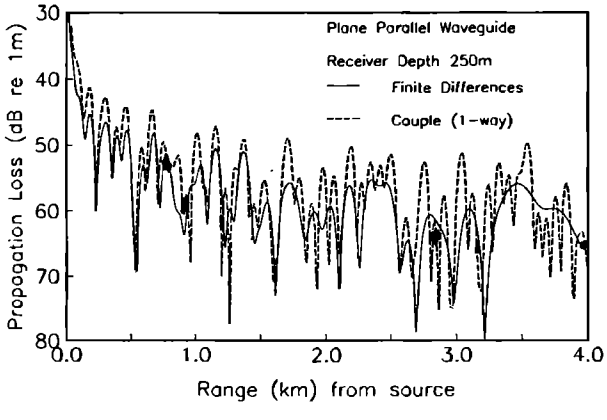

FIG. 9. Propagation-loss curve for the plane-parallel waveguide model.

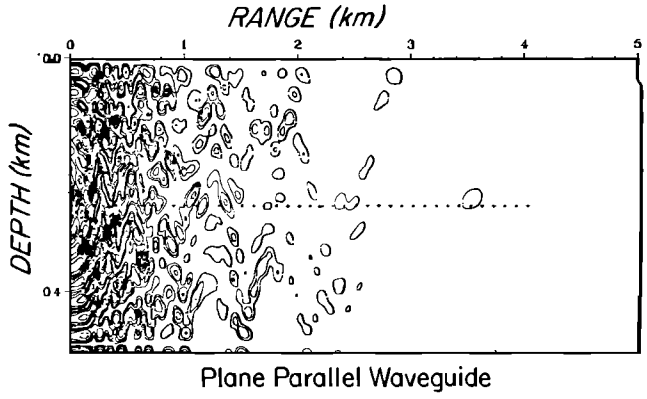

FIG. 10. Contoured-field solution for the plane-parallel waveguide model. Contour interval is 3 dB.

memory. They required 11 and 21 h of CPU time, respectively. We have run similar finite-difference codes on the Cyber 205 and Cray-XMP supercomputers and obtained another factor of 15 improvement over the VAX-8800. So, we estimate that these jobs would run on the supercomputers in 40 and 80 min, respectively.

The penetrable wedge was run on a microVAX-II office computer with 16 Mbytes of random-access (primary) memory and required 240 h of CPU time. Although this is clearly not the optimal way to work, it does demonstrate that the code can run effectively on general desk-top computers. As configured, this job ran in the background for 10 days while other office work and smaller finite-difference jobs were run in the foreground during the day. Although not very efficient in terms of "turn-around" time, it is reasonably cost effective since the microVAX was office equipment justified on the basis of an interactive work station. The ability to run large jobs in the background is an extra benefit at no additional cost.

For the benchmark problems, we removed the shear modulus terms from the wave equation to improve performance. Models with shear wave effects in the bottom would require longer computational times than those indicated above. However, shear waves excluded, the models above could be made more generally complex without increasing computational time. For example, we could add vertically and horizontally varying sound speed and/or density in the water column, including high-velocity inclusions. We could add an arbitrarily rough seafloor to the models. We could introduce velocity gradients (vertical and/or horizontal) to the subbottom in the penetrable-wedge case. We could add statistically varying velocity and density in the seafloor to look at the effects of scattering due to heterogeneity. All of these additional complexities can be added without increasing the cost or run time of the calculations.

IV. DISCUSSION

The finite-difference solution to the two-way wave equation provides good solutions to the acoustic-benchmark models. Although computationally more intensive than other methods, it has the flexibility to handle more generally complex media including shear-wave effects in the seafloor.

TABLE I. Numerical parameters and CPU times for benchmark solutions.

Test case	Δr (m)	Δz (m)	Δt (m/s)	Total range (m)	Total depth (m)	Total duration (s)	No. of stairsteps	Virtual memory allocated (M/bytes)	CPU time	Machine
Perfect wedge										
1	2.5	2.5	1.00	4,762.5	215	6.25	80	5.46	11 h 3min	VAX 8800
Lossless penetrable wedge										
2	2.5	2.5	1.00	4,125.0	500	6.25	80	10.63	239 h 16min.	microVAX
Plane parallel waveguide										
4a	2.5	2.5	0.83	5,000.0	500	3.33	N/A	13.02	20 h 52min	VAX 8800

The method also yields phase information for a given problem and if run for a pulse source, shows the energy partitioning of the wave field. Insight into the physical propagation effects can then be obtained, which is not offered by full continuous wave solutions. As yet, we have not implemented an effective way to handle large attenuations with the formulation, but the work of Day and Minster[14] describes a possible solution.

Since these models were run to longer times than are usually carried out, it may be necessary to go to finer grid spacings to obtain the best accuracy. Further computations should be carried out along these lines. Finer grid spacing would also represent the sloping bottom better in the wedge models.

The inaccuracy at low-propagation loss for the lower line of receivers in the penetrable wedge model was surprising. Further studies should be carried out to quantify this and minimize it.

We regard the comparison of techniques for benchmark models to be an extremely useful process: (i) Relatively minor coding errors can be detected and fixed; (ii) There is incentive to calibrate the code and produce output in a standard format; (iii) Comparison of codes can be readily made in terms of versatility, accuracy, computational effort, etc.; (iv) We can identify the range of parameters over which acceptable answers can be obtained; and (v) it provides a framework within which further work can be defined.

ACKNOWLEDGMENTS

This work was supported by the Office of Naval Research under Contract No. N00014-87-K-0007. Woods Hole Oceanographic Institution Contribution No. 7140.

[1]F. B. Jensen and C. M. Ferla, "Numerical solutions of range-dependent benchmark problems in ocean acoustics," J. Acoust. Soc. Am. **87**, 1499–1510 (1990).
[2]R. A. Stephen, "A comparison of finite difference and reflectivity seismograms for marine models," Geophys. J. R. Astron. Soc. **72**, 39–58 (1983).
[3]R. A. Stephen, "Finite difference seismograms for laterally varying marine models," Geophys. J. R. Astron. Soc. **79**, 184–198 (1984).
[4]M. E. Dougherty and R. A. Stephen, "Geoacoustic scattering from seafloor features in the ROSE area," J. Acoust. Soc. Am. **82**, 238–256 (1987).
[5]M. E. Dougherty and R. A. Stephen, "Seismic energy partitioning and scattering in laterally heterogeneous ocean crust," J. Pure Appl. Geophys. **128**, 195–229 (1988).
[6]R. A. Stephen, "A review of finite difference methods for seismo-acoustics problems at the sea floor," Rev. Geophys. **26**, 445–458 (1988).
[7]R. Madariaga, "Dynamics of an expanding circular fault," Bull. Seismol. Soc. Am. **66**, 639–666 (1976).
[8]J. Virieux, "*P*-wave propagation in heterogeneous media: velocity-stress finite-difference method," Geophysics **51**, 889–901 (1986).
[9]R. Clayton and B. Engquist, "Absorbing boundary conditions for acoustic and elastic wave equations," Bull. Seismol. Soc. Am. **67**, 1529–1540 (1977).
[10]A. R. Levander, "Use of the telegraphy equation to improve absorbing boundary efficiency for fourth-order acoustic wave finite difference schemes," Bull. Seismol. Soc. Am. **75**, 1847–1852 (1985).
[11]D. Cerjan, D. Kosloff, R. Kosloff, and M. Reshef, "A non-reflecting boundary condition for discrete acoustic and elastic wave equations," Geophysics **50**, 705–708 (1985).
[12]L. M. Nicoletis, "Simulation numerique de la propagation d'ondes sismiques dans les milieux stratifies a deux et trois dimensions: contribution a la construction et a l'interpretation des sismogrammes synthetiques," Ph.D. thesis, L'universite Pierre et Marie Curie—Paris VI (1981).
[13]A. Bamberger, G. Chavent, and P. Lailly, "Etude de schemas numeriques pour les equations de l'elastodynamique lineaire," Institute national de recherche en informatique et en automatique, Domaine de Voluceau, Rocquencourt, LeChesnay, France, Report No. 41 (1980).
[14]S. M. Day and J. B. Minster, "Numerical simulation of attenuated wavefields using a Pade approximant method," Geophys. J. R. Astron. Soc. **78**, 105–118 (1984).